Published in final edited form as:
Hum Mol Genet. 2003 December 1; 12(23): 3075–3086. doi:10.1093/hmg/ddg332.

Mouse models of USH1C and DFNB18: phenotypic and molecular analyses of two new spontaneous mutations of the *Ush1c* gene

Kenneth R. Johnson*, **Leona H. Gagnon**, **Lisa S. Webb**, **Luanne L. Peters**, **Norman L. Hawes**, **Bo Chang**, and **Qing Yin Zheng**
The Jackson Laboratory, Bar Harbor, ME 04609, USA

Abstract

We mapped two new recessive mutations causing circling behavior and deafness to the same region on chromosome 7 and showed they are allelic by complementation analysis. One was named ‘deaf circler’ (allele symbol *dfcr*) and the other ‘deaf circler 2 Jackson’ (allele symbol *dfcr-2J*). Both were shown to be mutations of the *Ush1c* gene, the mouse ortholog of the gene responsible for human Usher syndrome type IC and for the non-syndromic deafness disorder DFNB18. The *Ush1c* gene contains 28 exons, 20 that are constitutive and eight that are alternatively spliced. The *dfcr* mutation is a 12.8 kb intragenic deletion that eliminates three constitutive and five alternatively spliced exons. The *dfcr-2J* mutation is a 1 bp deletion in an alternatively spliced exon that creates a transcriptional frame shift, changing 38 amino acid codons before introducing a premature stop codon. Both mutations cause congenital deafness and severe balance deficits due to inner ear dysfunction. The stereocilia of cochlear hair cells are disorganized and splayed in mutant mice, with subsequent degeneration of the hair cells and spiral ganglion cells. Harmonin, the protein encoded by *Ush1c*, has been shown to bind, by means of its PDZ-domains, with the products of other Usher syndrome genes, including *Myo7a*, *Cdh23* and *Sans*. The complexes formed by these protein interactions are thought to be essential for maintaining the integrity of hair cell stereocilia. The *Ush1c* mutant mice described here provide a means to directly investigate these interactions *in vivo* and to evaluate gene structure–function relationships that affect inner ear and eye phenotypes.

INTRODUCTION

As part of our research program at The Jackson Laboratory to identify genes causing hearing impairment in mice, we have been selecting and studying mutant mice that exhibit circling or head tossing behavior. This behavior is characteristic of vestibular dysfunction of the inner ear and often is associated with deafness. We mapped two new recessive mutations causing such circling behavior and deafness to the same region on chromosome (Chr) 7. The two independently occurring mutations were shown to be allelic by complementation analysis. The one first discovered was named ‘deaf circler’ (allele symbol *dfcr*), and the other was given the name ‘deaf circler 2 Jackson’ (allele symbol *dfcr-2J*), in accordance with nomenclature guidelines. In this paper we describe the phenotypes of these two new spontaneous mutations and show that both are mutations of the *Ush1c* gene, the mouse ortholog of the gene responsible for human Usher syndrome type IC and the non-syndromic deafness disorder DFNB18.

The Usher syndromes are a genetically heterogeneous group of recessive disorders that cause both deafness and blindness. They can be divided clinically into three subtypes based on the severity and progression of associated deafness, vestibular dysfunction, and retinitis

*To whom correspondence should be addressed. Tel: +1 2072886228; Fax: +1 2072886149; krj@jax.org.

pigmentosa (RP). Usher syndrome type I (USH1), the most severe form, is characterized by profound congenital sensory deafness, vestibular dysfunction, and progressive RP with onset by age 10. With the inclusion of the *Ush1c* mouse mutations described in this paper, mouse models now exist for all five of the known USH1 genes (Table 1). USH1C is a subtype of Usher syndrome type I that was localized to Chromosome 11 by linkage analysis of Acadian families in Louisiana (1,2). It was later shown to be caused by mutations in a gene designated *USH1C*, which encodes a PDZ-domain-containing protein named harmonin (3,4). Mutations of this same gene are also responsible for the non-syndromic recessive disorder DFNB18 (5–7).

The *USH1C* gene is composed of 28 exons, including 20 that are constitutive and 8 that are alternatively spliced in the mouse (4). These alternative transcripts encode multiple harmonin isoforms, including two type ‘a’ isoforms, which are the most abundant and widely expressed, and three longer type ‘b’ isoforms, which are more restricted in their tissue distribution. The human protein also exhibits multiple tissue-specific isoforms (8). The lack of RP in DFNB18 patients was attributed to the nature of the *USH1C* mutations, which occurred in the alternatively spliced exons that encode the longer harmonin b isoforms expressed in the inner ear but not the eye (6).

The two new *Ush1c* mutants described in this paper provide important mouse models for studying the pathogenesis and potential therapies for human USH1C. One of the mutations is a large deletion that includes both constitutive and alternatively spliced exons and alters both a and b isoforms; the other causes a frame-shift in one of the alternatively transcribed exons and alters only b isoforms. These qualitatively different mutations provide a means to evaluate the functional domains of the *Ush1c* gene. The mutations also will be valuable for identifying molecular pathways and gene interactions important in hearing and vision. The *Ush1c* gene product, harmonin, is thought to interact, by means of its PDZ-binding domain, with the products of three other Usher syndrome genes, *Myo7a*, *Cdh23*, and *Sans* (9–11). PDZ-domains are known to facilitate protein complex assembly at particular subcellular locations, especially at the plasma membrane (12,13). The *Ush1c* mutant mice described here can be used to directly investigate these molecular interactions *in vivo*, by producing and analyzing mice with compound mutations.

RESULTS

Origins and genetic mapping of *dfcr* and *dfcr-2J*

The *dfcr* mutation arose spontaneously at The Jackson Laboratory in a strain with a predominantly BALB/cByJ background (see Materials and Methods). The *dfcr-2J* mutation arose spontaneously in a stock derived from 129S4/SvJae ES cells and C57BL/6J mice that carries a targeted mutation of beta adducin, *Add2* (14). The mutant strain has been crossed and maintained so that it no longer contains the *Add2* targeted mutation.

All *dfcr* and *dfcr-2J* mutants exhibit head tossing and hyperactive circling behavior and are unable to swim. These phenotypes are inherited as recessive traits with full penetrance in homozygotes. Because of their similar phenotypes and map locations (see below), we tested the two mutations for allelism by complementation analysis. Two matings between pairs of homozygous mice (*dfcr*/*dfcr* × *dfcr-2J*/*dfcr-2J*) produced a total of nine progeny all with mutant phenotypes, confirming that the two mutations were allelic. Both mutant male and mutant female (*dfcr*/*dfcr* and *dfcr-2J*/*dfcr-2J*) mice have normal life spans and can breed.

By linkage intercrosses with CAST/Ei, we mapped the *dfcr* and *dfcr-2J* mutations to the same location on Chr-7. Analysis of 54 F2 mice (108 meioses) positioned *dfcr* between *D7Mit157* (3.7% recombination) and *D7Mit272* (1.9% recombination), non-recombinant with

D7Mit158. Analysis of 93 F2 mice (186 meioses) placed the *dfcr 2J* mutation between *D7Mit228* (4.8% recombination) and *D7Mit145* (5.4% recombination), non-recombinant with *D7Mit229*, *D7Mit69* and *D7Mit230*.

Candidate genes

The map location of *dfcr* and *dfcr-2J* suggested they might be mutations of the otogelin gene (*Otog*), which is located within the genetically defined intervals containing these mutations (Fig. 1). Mice with targeted mutations of *Otog* (15) and mice with the spontaneous twister (*twt*) mutation of *Otog* (16) have vestibular and hearing impairment similar to *dfcr* and *dfcr-2J* mutants. To test for allelism, we set up a mating between a homozygous *dfcr*/*dfcr* female and a homozygous twister ($Otog^{twt}/Otog^{twt}$) male. All five offspring from this cross exhibited normal hearing and behavior; therefore, we concluded that *dfcr* is not a mutation of *Otog*.

The *Ush1c* gene is also located in the *dfcr* and *dfcr-2J* candidate regions, less than 10 kb from *Otog* (Fig. 1). No mouse mutations of *Ush1c* have been reported, but human mutations of *USH1C* underlie both syndromic (Usher syndrome type IC) and non-syndromic (DFNB18) deafness disorders (3–6). Because of the map location and association with deafness in humans, we next considered *Ush1c* as a likely candidate for the *dfcr* and *dfcr-2J* mutations.

We designed gene-specific probes for Southern blots and PCR primers for genomic and cDNA sequence analyses according to the mouse *Ush1c* cDNA sequences in GenBank (accession numbers NM_023649 and AY103465) and the exon–intron structure and nomenclature described by Verpy et al. (4). Intronic DNA sequences were obtained from the public mouse genome sequence (Ensembl Gene ID ENSMUSG00000030838). The DNA sequences of all PCR primers used in this study are given in Table 2.

Molecular characterization of the *dfcr* and *dfcr-2J* mutations

Genomic DNA from *dfcr* and *dfcr-2J* mutant mice and their controls was examined for gross alterations in the *Ush1c* gene by Southern blot analysis. DNA from *dfcr-2J* mutant mice gave the same *Ush1c* restriction fragment lengths as wild-type control mice for all restriction enzymes and probes used. DNA from *dfcr* mutant mice, however, showed altered sizes or missing fragments when hybridized with probes containing *Ush1c* exons 12, 13, 14, 15, A, B, C or D (Fig. 2A). PCR primers flanking these same exons failed to amplify products from genomic DNA of *dfcr*/*dfcr* mice, but amplified the expected-sized products from DNA of wild-type control and *dfcr-2J*/*dfcr-2J* mice (Fig. 2B). These results indicate that the *dfcr* mutation is a large deletion of *Ush1c* including exons 12-D.

We designed PCR primers (in11-F and inD-R; Table 2) on either side of the deleted region and sequenced the resulting product from *dfcr*/*dfcr* genomic DNA. The DNA sequence exactly matched the mouse *Ush1c* gene sequence (Ensembl Gene ID ENSMUSG00000030838) from the forward primer position in intron 11 through the first 25 bp of exon 12; it then skipped to a position 110 bp past the 3′ end of exon D and continued to the position of the reverse primer in intron D. This result indicates that 12 770 bp are deleted in the mutant DNA, including 118 bp from exon 12 and exons 13, 14, 15, A, B, C and D. No other genomic rearrangements were detected that are associated with this deletion.

The *dfcr-2J* mutation was not detected by Southern blot analysis, so the DNA sequence of all 28 *Ush1c* exons and their splice junctions was compared between mutant mice and +/+ controls. PCR primers flanking each exon (Table 2) were designed to amplify genomic DNA for sequence analysis. The only sequence difference detected was a 1 bp deletion at position 4 of exon C in mutant DNA (Fig. 3A). The deletion creates a transcriptional frame shift that changes

the codons for 38 amino acids before introducing a stop codon at the beginning of exon D (Fig. 3B). DNA from two additional *dfcr-2J*/*dfcr-2J* mutant mice was sequenced to confirm this 1 bp deletion, which was not observed in DNA from any of the inbred strains we examined (C57BL/6J, 129S1/SvImJ or BALB/cByJ), nor in any of the Genbank database entries for mouse, rat, or human genomic DNA, mRNAs, or ESTs.

Effects of the *Ush1c* mutations on transcription and translation

The mouse *Ush1c* gene consists of 28 exons spanning more than 43 kb of genomic DNA. Eight of the 28 exons are alternatively spliced: exons 15, A, B, C, D, E, F, and G (4). These alternative transcripts encode multiple harmonin isoforms, including two type a isoforms, which are the most abundant and widespread forms and usually include exon 15. Three type b isoforms are more restricted in their tissue distribution and include exons A, B, C, D, E, F and sometimes G or G′. Transcripts containing exons A–F and exon G/G′ appear to be expressed only in the inner ear. The exon–intron structure of the *Ush1c* gene and the positions of the *dfcr* and *dfcr-2J* mutations are diagramed in Figure 4A.

To evaluate how the *dfcr* and *dfcr-2J* mutant genes are transcribed, RNA was extracted from mutant and control mice and converted to cDNA for PCR analysis. *Ush1c* transcripts were detected in *dfcr*/*dfcr* and *dfcr-2J*/*dfcrf-2J* mice in all tissues examined (eye, inner ear, brain, kidney and intestine); results for inner ear and kidney are shown in Figure 4B. The RT–PCR product sizes from *dfcr-2J*/*dfcrf-2J* mice were the same as those from control mice for all *Ush1c* regions examined. Transcript size is not be affected by the *dfcr-2J* mutation, but the translated protein would be altered as described above (Fig. 3B).

For *dfcr*/*dfcr* mutants, primers corresponding to DNA sequences located 5′ of the deletion (Fig. 4B) gave the same sized products as controls, whereas primers that spanned the deleted region amplified smaller products (Fig. 4C). Sequence analysis of the mutant 574 bp PCR product (Fig. 4C, lanes 1 and 2) that was amplified with primers specific to exons 10 and 21 revealed an in-frame splicing of exon 11 with exon 16. This mutant transcript, present in all tissues examined, lacks exons 12, 13, 14 and 15 (396 nt), which encode 132 of the 548 amino acids of harmonin isoform a1 (4). Sequence analysis of a faint ~700 bp PCR product amplified from inner ear cDNA of *dfcr*/*dfcr* mice with primers specific to exon 10 and exon G (Fig. 4D) revealed an in-frame splicing of exon 11 with exon E. This mutant inner ear-specific transcript lacks exons 12, 13, 14, A, B, C and D (1137 nt), which encode 379 of the 852–910 amino acids of harmonin isoform b (4). The *dfcr* mutant splice forms do not change the normal reading frame of the *Ush1c* transcripts and, therefore, do not introduce any new amino acid or stop codons.

Inner ear pathology

The vestibular dysfunction of mutant mice suggested that they might also be hearing impaired. We assessed hearing in mutant and control mice by auditory-evoked brainstem response (ABR) thresholds to broad-band clicks and to 8, 16 and 32 kHz pure-tone stimuli (Table 3), according to previously established criteria (17). ABR tests of eight homozygous *dfcr* mutants (one tested at 21 days, four at 32 days, and three at 57 days of age) indicated they were completely deaf (no detectable ABR with 100 dB SPL stimuli), whereas seven heterozygotes (one tested at 21 days, two at 32 days, two at 88 days and two at 176 days of age) had ABR thresholds in the normal-hearing range. Two mice homozygous for the *dfcr-2J* mutation were tested by ABR analysis at 98 days of age and found to be completely deaf, whereas four age-matched heterozygotes had normal hearing.

The deafness and balance impairment of mutant mice indicated an inner ear dysfunction. We therefore examined whole mounts and cross sections of inner ears from mutant and control

mice by light microscopy and organ of Corti surface preparations by scanning electron microscopy (SEM). Careful examinations of whole mounts of inner ears from adult mice revealed no discernable morphological abnormalities. Examinations of cross sections through the cochleae of both *dfcr*/*dfcr* and *dfcr-2J*/*dfcr-2J* mutant mice revealed a progressive loss of hair cells and a secondary loss of spiral ganglion cells. At 3 months of age, mutant cochleae already exhibited noticeable hair cell degeneration, especially in the basal and middle turns. By 8 months of age there was severe degeneration of hair cells, and spiral ganglion cell loss was apparent (Fig. 5). Degeneration appeared specific to the hair cells and not to the supporting cells of the organ of Corti. All other cochlear structures, including Reissner's membrane and stria vascularis, appeared normal in mutant mice.

The *Ush1c* mutant mice are congenitally deaf (at least by 21 days, the earliest age tested by ABR), but hair cell degeneration was not apparent in cochlear cross sections until much later, indicating that hair cell dysfunction preceded degeneration. To examine earlier indicators of hair cell dysmorphology that might be associated with dysfunction, we examined surface preparations of the organ of Corti by SEM, with particular attention to the stereocilia (Fig. 6). At 3 weeks of age, outer hair cell stereocilia of both *dfcr*/*dfcr* and *dfcr-2J*/*dfcr-2J* mutant mice appeared disorganized and splayed compared with the well-organized pattern and rigid structure typical of normal stereocilia. Stereocilia of inner hair cells of mutant mice also showed a disorganized appearance, but less so than that of outer hair cells.

SEM analysis of the 3-week-old mouse cochleae revealed a degree of hair cell loss that was not apparent by light microscopic examination of cross sections at this age. The expansion of supporting cells into the regions previously occupied by degenerated hair cells disrupts the positions of the remaining hair cells and results in the disorganized pattern of hair cells seen in Figure 6. This scarring process seals the reticular lamina, thus maintaining the barrier between endolymph and perilymph (18).

The circling and head tossing behaviors of the *dfcr* and *dfcr-2J* mutant mice are probably caused by similar hair cell defects in the vestibular end organs of the inner ear. These structures were not examined in this study but will be the focus of future investigation.

Eye phenotype

We examined the eyes of *Ush1c* mutant mice because mutations of the homologous gene in humans cause progressive retinitis pigmentosa. The eyes of *dfcr*/*dfcr* and *dfcr-2J*/*dfcr-2J* mutant mice appear clinically normal on gross examination, having a normal fundus with thin retinal vessels at 1 and 8 months of age, the same as littermate controls. ERGs of eyes from homozygous *dfcr* and *dfcr-2J* mutants appeared normal compared with those of heterozygous littermate controls at 9 months of age.

Histological examination of eyes from both *dfcr* and *dfcr-2J* mutant homozygotes showed no gross abnormalities; however, a slight peripheral retinal degeneration was noticed in the three homozygous *dfcr* mutants that were examined at 9 months of age, but not in three littermate controls (Fig. 7). The *dfcr-2J* homozygous mutants had normal retinas at that age.

DISCUSSION

The *dfcr* mutation is a large deletion that includes both constitutive and alternatively spliced exons, whereas the *dfcr-2J* mutation causes a frame-shift in a single alternatively transcribed exon. These qualitatively different mutations provide a means to evaluate the functional domains of the *Ush1c* gene and the harmonin isoforms it encodes. Alternative splicing of the *Ush1c* gene results in multiple harmonin isoforms (4). The short isoform a transcripts are the most abundant and are present in most tissues. The inner ear is one of the few tissues that

express the longer isoform b transcripts, particularly those that include exon G. Both isoform a and isoform b transcripts are affected by the *dfcr* deletion; however, the *dfcr-2J* mutation affects only isoform b transcripts. The deafness and vestibular dysfunction that is common to both mutations, therefore, must be the result of altered isoform b transcripts, emphasizing the importance of this harmonin isoform to normal inner ear function. Isoform b contains a PST (proline, serine, threonine-rich) domain that is not present in isoform a. This PST region may be critical for the F-actin binding property of harmonin b and thus may help to stabilize the actin fibers in hair cell stereocilia (9).

The *dfcr* mutation, though more severe than *dfcr-2J*, may not be completely null. Altered harmonin isoforms retaining partial function might be translated from *dfcr* mutant transcripts. The reading frames are not changed in the shortened *dfcr* transcripts of either isoform a or isoform b, and transcription proceeds to the normal stop codons (Fig. 4A). The exons deleted by the *dfcr* mutation in isoform a transcripts encode the first coiled coil (CC1) domain of harmonin, and the exons deleted in the mutant isoform b transcripts encode the two coiled-coil domains (CC1 and CC2) and the PST domain of harmonin. None of the three PDZ-encoding domains are deleted in *dfcr* mutant transcripts, but if translated the spatial relationships of these domains would be altered in mutant proteins, with possible functional significance.

The presence of RP in USH1C and its absence in DFNB18 has been attributed to the nature of the underlying *USH1C* mutations (6). All of the *USH1C* mutations that cause type I Usher syndrome (3,4,19) have occurred in constitutive exons that are expressed in both eye and cochlea of mice (4), whereas mutations in alternatively transcribed exons that are not expressed in the eye have been associated with nonsyndromic deafness (6). If the same relationship held for mutant *Ush1c* phenotypes in the mouse, we would expect the *dfcr* mutation to cause both deafness and retinal degeneration (because it affects all transcripts) and the *dfcr-2J* mutation to cause only deafness (because it affects isoform b transcripts found in the inner ear but not the eye). We found no gross retinal abnormalities or ERG evidence for retinal dysfunction in *dfcr* mutants, which indicates that mutational disruption of constitutive *Ush1c* exons is not sufficient to cause this pathology in the mouse. Mouse mutations in other Usher syndrome-related genes (*Myo7a*, *Cdh23*, *Pcdh15* and *Sans*), even those presumed to be null, also lack retinal phenotypes (20–23), suggesting a species difference in manifestation. However, upon more refined analyses, some physiological anomalies recently have been detected in the retinas of mice with *Myo7a* mutations (24,25). Subtle retinal abnormalities may also occur in the other mouse models of Usher syndromes, including *dfcr* mutant mice. Indeed, we found some histological evidence of a slight peripheral degeneration in 9-month-old *dfcr* mutants (Fig. 7). It is not clear if this peripheral degeneration is caused by the *dfcr* mutation or by a natural aging process including light toxicity, since the *dfcr* mutation is carried on a BALB/cBy albino background. However, because the degeneration was not seen in BALB/cBy littermate controls, the association of this retinal pathology with the *dfcr* mutation warrants further investigation.

In the inner ear of the mouse, the *Ush1c* gene is expressed only in sensory hair cells (4), consistent with the cochlear abnormalities we observed for *dfcr* and *dfcr-2J* mutants (Fig. 5). The abnormal stereocilia morphology observed in the *Ush1c* mutant mice (Fig. 6) is similar to that reported in mice with mutations of *Myo7a* (26), *Cdh23* (20), *Pcdh15* (22), and *Sans* (23), which are models for other forms of human USH1 (Table 1). The products of these genes may form a functional network that maintains stereocilia cohesion (9–11). Disruption of this network would result in disorganization of the hair bundle and the splayed stereocilia seen in mutant mice. The PDZ-domains of harmonin are thought to be of central importance to the formation and maintenance of this transmembrane complex. In particular, the harmonin isoform b, and not a, was shown to interact with the actin cytoskeleton and to bind with cadherin 23 and myosin VIIa (9). Harmonin isoform a (which is expressed in most tissues, including

the eye) is altered by the *dfcr* mutation but not by the *dfcr-2J* mutation. Harmonin isoform b (which is expressed in the inner ear but not the eye) is disrupted by both mutations. The mouse *Ush1c* mouse mutants, thus, will provide a direct means to examine the roles of the different harmonin isoforms in these interactive relationships.

MATERIALS AND METHODS

Mice

All mice were from production or research facilities of The Jackson Laboratory, and all procedures were approved by the institutional Animal Care and Use Committee. Both the *dfcr* and the *dfcr-2J* mutations arose spontaneously at The Jackson Laboratory. The *dfcr* mutation occurred in the CBySmn.CB17-*Prkdc*^{scid}/J strain. It was then backcrossed twice to BALB/cByJ to remove the *scid* mutation from the strain prior to maintaining by sibling matings. The *dfcr-2J* mutation arose in a mixed 129;B6 colony segregating a targeted mutation of the beta adducin 2 gene (*Add2*) and since has been crossed and maintained so that it no longer contains the *Add2* mutant allele.

Preparation of genomic DNA, RNA and cDNA

Genomic DNA for genotyping mice was rapidly prepared from tail tips by the hot sodium hydroxide and Tris (Hot SHOT) procedure (27). High-quality genomic DNA for mutation screening was prepared from mouse spleens by standard phenol/chloroform extraction and ethanol precipitation methods. Total RNA was purified from adult mouse eye inner ear, brain, kidney and intestines with TRIzol reagent, according to manufacturer's protocol (Invitrogen Corp., Carlsbad, CA, USA). DNA and RNA concentrations were estimated by spectrophotometric measurements of absorbance. Mouse cDNA was prepared from total RNA extracted with the SuperScript First Strand cDNA Synthesis System for RT–PCR (Invitrogen Corp., Carlsbad, CA, USA).

Genetic mapping

PCR primer pairs (MapPairs) for MIT microsatellite markers distributed throughout the mouse genome (28) were purchased from Research Genetics (Huntsville, AL, USA) or from Integrated DNA Technologies (Coralville, IA, USA). PCR reactions were composed of 50 ng genomic DNA in 10 μl containing 50mM KCL, 10mM Tris–HCL (pH 9.0 at 25°C), and 0.01% Triton-X-100, 2.25mM $MgCl_2$, 100 nM of each primer (forward and reverse), 100 μM of each of four deoxyribonucleoside triphosphates, and 1.0 units of *Taq* DNA polymerase (Amplitaq from Applied Biosystems no. N808-0145). Amplification consisted of one cycle of denaturation at 97°C for 30 s followed by 40 cycles, each consisting of 94°C for 30 s, denaturation, 55°C for 30 s of annealing, and 72°C for 30 + 1 s per cycle of extension. After the 40 cycles, the final product was extended for 10 min at 72°C. A pooled DNA strategy (29) was used to efficiently localize the mutations to Chr 7, and then individual DNAs were typed to refine the map position. Gene order, determined by minimizing the number of obligate crossover events, and recombination frequency estimates were calculated with the aid of the Map Manager computer program (30).

Mutation screening

PCR primers used to amplify portions of the mouse *Ush1c* gene for sequence comparisons are given in Table 2. PCR conditions were the same as described above for genetic mapping except that reaction volumes were 25 μl rather than 10 μl. PCR-amplified products from cDNA and genomic DNA templates were purified with the QIAquick PCR Purification Kit (Qiagen Inc., Valencia, CA, USA). DNA was sequenced using an Applied Biosystems 373A DNA

Sequencer and an optimized DyeDeoxy Terminator Cycle Sequencing method. The same primers used for PCR amplification were also used for cycle sequencing.

For Southern blot analysis, DNA probes for specific regions of the *Ush1c* gene were generated by PCR amplification of genomic DNA from BALB/cByJ mice with the primers listed in Table 2. The PCR fragments were separated on agarose gels, extracted and purified with the QIAquick Gel Extraction Kit (Qiagen, Inc., Valencia, CA, USA). Preparation of Southern blots, probe labeling, and hybridization methods followed previously described procedures (31).

Assessment of hearing by ABR

Briefly, mice are anesthetized and body temperature is maintained at 37–38°C by placing them on an isothermal pad in a sound-attenuating chamber. Sub-dermal needles are used as electrodes, inserted at the vertex, and ventrolaterally to each ear. Stimulus presentation, ABR acquisition, equipment control and data management are coordinated using the computerized Intelligent Hearing Systems (IHS; Miami, FL, USA). A pair of high frequency transducers is coupled with the IHS system to generate specific acoustic stimuli. Clicks, and 8, 16 and 32 kHz tone-bursts are respectively channeled through plastic tubes into the animal's ear canals. The amplified brainstem responses are averaged by a computer and displayed on the computer screen. Auditory thresholds are obtained for each stimulus by reducing the sound pressure level (SPL) at 10 dB steps and finally at 5 dB steps up and down to identify the lowest level at which an ABR pattern can be recognized.

Histological analyses of inner ears

Anesthetized mice were perfused through the left ventricle of the heart with phosphate-buffered saline (PBS) followed by Bouin's fixative. For microscopic analysis of cross-sections, inner ears from mutant and control mice were dissected, perfused with Bouin's fixative, immersed in same for 24–48 h, decalcified with Cal-EX solution for 6 h, and embedded in paraffin. Sections (7 μm) were cut, mounted on glass slides and counterstained in hematoxylin/eosin (H&E).

For SEM analysis, eight inner ears from mutant mice and six ears from controls were dissected and fixed in 2.5% glutaraldehyde, 0.25% tannic acid, in 0.1M phosphate buffer (pH 7.2) for 5 h at 4°C. The temporal bone surrounding the cochlea and the tectorial membrane were removed to expose the organ of Corti. An osmium tetroxide–thiocarbohydrazide (OTOTO) procedure was used to stain prior to dehydrating and critical-point drying. Specimens were sputter coated with gold and examined at 15 kV under a Hitachi 3000N scanning electron microscope.

Clinical evaluation of eyes and electroretinography

All mice had pupils dilated with 1% atropine ophthalmic drops and were evaluated by indirect ophthalmoscopy with a 78 diopter lens. Signs of retinal degeneration, such as vessel attenuation, alterations in the RPE, and presence or absence of retinal dots were noted (32).

Methods for ERG were as previously described (33). After at least 2 h of dark-adaptation, mice were anesthetized with an intraperitoneal injection of normal saline solution containing ketamine (15 mg/g) and xylazine (7 mg/g body wt). Electroretinograms (ERGs) were recorded from the corneal surface of one eye after pupil dilation (1% atropine sulfate) using a gold loop electrode referenced to a gold wire in the mouth. A needle electrode placed in the tail served as ground. A drop of methylcellulose (2.5%) was placed on the corneal surface to ensure electrical contract and to maintain corneal integrity. Body temperature was maintained at a constant temperature of 38°C using a heated water pad. All stimuli were presented in a Ganzfeld dome (LKC Technologies, Gaithersburg, MD, USA) whose interior surface was painted with a highly reflective white matte paint (no. 6080; Eastman Kodak, Rochester, NY, USA). Stimuli

were generated with a Grass Photic Stimulator (model PS33 Plus; Grass Instruments, Worcester, MA, USA) affixed to the outside of the dome at 90μ to the viewing porthole. Rod-dominated responses were recorded to short-wavelength (λ_{max} = 470 nm; Wratten 47A filter) flashes of light over a 4.0 log unit range of intensities (0.3 log unit steps) up to the maximum allowable by the photic stimulator. Cone-dominated responses were obtained with white flashes (0.3 steps) on the rod-saturating background after 10 min of exposure to the background light to allow complete light adaptation. Responses were amplified (Grass CP511 AC amplifier, ×10 000; 3 dB down at 2 and 10 000 Hz) and digitized using an I/O board (model PCI-1200; National Instruments, Austin, TX, USA) in a personal computer. Signal processing was performed with custom software (LabWindows/CVI; National Instruments). Signals were sampled every 0.8 ms over a response window of 200 ms. For each stimulus condition, responses were computer-averaged with up to 50 records averaged for the weakest signals. A signal rejection window could be adjusted online to eliminate electrical artifacts.

Histological and electron microscopy of eyes

A total of 10 eyes were studied histologically. The eyes for light microscopy were immediately removed and immersed in cold fixative (1% paraformaldehyde, 2% glutaraldehyde, and 0.1M cacodylate buffer). Eyes were left in fixative for 24 h, after which time they were transferred to cold 0.1M cacodylate buffer solution for an additional 24 h. Samples were embedded in methacrylate historesin, and sections were cut and stained with hematoxylin and eosin (H&E) according to previously published methods (33).

Acknowledgments

We thank Verity Letts and Richard Libby for critical review of this manuscript, Heping Yu for technical expertise in ABR measurements, Peter Finger for EM imaging assistance, Sandra Gray for husbandry skills and A. Sawyer for initially identifying the *dfcr* mutant mouse. This work was supported by National Institutes of Health (NIH) grants DC62108, DC04301, DC04376, EY07758, RR01183, DK07449 and HL64885. TJL institutional shared services are supported by NIH grant CA34196.

REFERENCES

1. Keats BJ, Nouri N, Pelias MZ, Deininger PL, Litt M. Tightly linked flanking microsatellite markers for the Usher syndrome type I locus on the short arm of chromosome 11. Am. J. Hum. Genet 1994;54:681–686. [PubMed: 8128966]
2. Smith RJ, Lee EC, Kimberling WJ, Daiger SP, Pelias MZ, Keats BJ, Jay M, Bird A, Reardon W, Guest M, et al. Localization of two genes for Usher syndrome type I to chromosome 11. Genomics 1992;14:995–1002. [PubMed: 1478678]
3. Bitner-Glindzicz M, Lindley KJ, Rutland P, Blaydon D, Smith VV, Milla PJ, Hussain K, Furth-Lavi J, Cosgrove KE, Shepherd RM, et al. A recessive contiguous gene deletion causing infantile hyperinsulinism, enteropathy and deafness identifies the Usher type 1C gene. Nat. Genet 2000;26:56–60. [PubMed: 10973248]
4. Verpy E, Leibovici M, Zwaenepoel I, Liu XZ, Gal A, Salem N, Mansour A, Blanchard S, Kobayashi I, Keats BJ, et al. A defect in harmonin, a PDZ domain-containing protein expressed in the inner ear sensory hair cells, underlies Usher syndrome type 1C. Nat. Genet 2000;26:51–55. [PubMed: 10973247]
5. Ahmed ZM, Smith TN, Riazuddin S, Makishima T, Ghosh M, Bokhari S, Menon PS, Deshmukh D, Griffith AJ, Friedman TB, et al. Nonsyndromic recessive deafness DFNB18 and Usher syndrome type IC are allelic mutations of USHIC. Hum. Genet 2002;110:527–531. [PubMed: 12107438]
6. Ouyang XM, Xia XJ, Verpy E, Du LL, Pandya A, Petit C, Balkany T, Nance WE, Liu XZ. Mutations in the alternatively spliced exons of USH1C cause non-syndromic recessive deafness. Hum. Genet 2002;111:26–30. [PubMed: 12136232]
7. Jain PK, Lalwani AK, Li XC, Singleton TL, Smith TN, Chen A, Deshmukh D, Verma IC, Smith RJ, Wilcox ER. A gene for recessive nonsyndromic sensorineural deafness (DFNB18) maps to the

chromosomal region 11p14-p15.1 containing the Usher syndrome type 1C gene. Genomics 1998;50:290–292. [PubMed: 9653658]

8. Scanlan MJ, Williamson B, Jungbluth A, Stockert E, Arden KC, Viars CS, Gure AO, Gordan JD, Chen YT, Old LJ. Isoforms of the human PDZ-73 protein exhibit differential tissue expression. Biochim. Biophys. Acta 1999;1445:39–52. [PubMed: 10209257]
9. Boeda B, El-Amraoui A, Bahloul A, Goodyear R, Daviet L, Blanchard S, Perfettini I, Fath KR, Shorte S, Reiners J, et al. Myosin VIIa, harmonin and cadherin 23, three Usher I gene products that cooperate to shape the sensory hair cell bundle. EMBO J 2002;21:6689–6699. [PubMed: 12485990]
10. Siemens J, Kazmierczak P, Reynolds A, Sticker M, Littlewood-Evans A, Muller U. The Usher syndrome proteins cadherin 23 and harmonin form a complex by means of PDZ-domain interactions. Proc. Natl Acad. Sci. USA 2002;99:14946–14951. [PubMed: 12407180]
11. Weil D, El-Amraoui A, Masmoudi S, Mustapha M, Kikkawa Y, Laine S, Delmaghani S, Adato A, Nadifi S, Zina ZB, et al. Usher syndrome type I G (USH1G) is caused by mutations in the gene encoding SANS, a protein that associates with the USH1C protein, harmonin. Hum. Mol. Genet 2003;12:463–471. [PubMed: 12588794]
12. Sheng M, Sala C. PDZ domains and the organization of supramolecular complexes. Annu. Rev. Neurosci 2001;24:1–29. [PubMed: 11283303]
13. Fanning AS, Anderson JM. PDZ domains: fundamental building blocks in the organization of protein complexes at the plasma membrane. J. Clin. Invest 1999;103:767–772. [PubMed: 10079096]
14. Gilligan DM, Lozovatsky L, Gwynn B, Brugnara C, Mohandas N, Peters LL. Targeted disruption of the beta adducin gene (Add2) causes red blood cell spherocytosis in mice. Proc. Natl Acad. Sci. USA 1999;96:10717–10722. [PubMed: 10485892]
15. Simmler MC, Cohen-Salmon M, El-Amraoui A, Guillaud L, Benichou JC, Petit C, Panthier JJ. Targeted disruption of otog results in deafness and severe imbalance. Nat. Genet 2000;24:139–143. [PubMed: 10655058]
16. Simmler MC, Zwaenepoel I, Verpy E, Guillaud L, Elbaz C, Petit C, Panthier JJ. Twister mutant mice are defective for otogelin, a component specific to inner ear acellular membranes. Mamm. Genome 2000;11:960–966. [PubMed: 11063250]
17. Zheng QY, Johnson KR, Erway LC. Assessment of hearing in 80 inbred strains of mice by ABR threshold analyses. Hear. Res 1999;130:94–107. [PubMed: 10320101]
18. Raphael Y. Cochlear pathology, sensory cell death and regeneration. Br. Med. Bull 2002;63:25–38. [PubMed: 12324382]
19. Zwaenepoel I, Verpy E, Blanchard S, Meins M, Apfelstedt-Sylla E, Gal A, Petit C. Identification of three novel mutations in the USH1C gene and detection of thirty-one polymorphisms used for haplotype analysis. Hum. Mutat 2001;17:34–41. [PubMed: 11139240]
20. Di Palma F, Holme RH, Bryda EC, Belyantseva IA, Pellegrino R, Kachar B, Steel KP, Noben-Trauth K. Mutations in Cdh23, encoding a new type of cadherin, cause stereocilia disorganization in waltzer, the mouse model for Usher syndrome type 1D. Nat. Genet 2001;27:103–107. [PubMed: 11138008]
21. Gibson F, Walsh J, Mburu P, Varela A, Brown KA, Antonio M, Beisel KW, Steel KP, Brown SD. A type VII myosin encoded by the mouse deafness gene shaker-1. Nature 1995;374:62–64. [PubMed: 7870172]
22. Alagramam KN, Murcia CL, Kwon HY, Pawlowski KS, Wright CG, Woychik RP. The mouse Ames waltzer hearing-loss mutant is caused by mutation of Pcdh15, a novel protocadherin gene. Nat. Genet 2001;27:99–102. [PubMed: 11138007]
23. Kikkawa Y, Shitara H, Wakana S, Kohara Y, Takada T, Okamoto M, Taya C, Kamiya K, Yoshikawa Y, Tokano H, et al. Mutations in a new scaffold protein Sans cause deafness in Jackson shaker mice. Hum. Mol. Genet 2003;12:453–461. [PubMed: 12588793]
24. Gibbs D, Kitamoto J, Williams DS. Abnormal phagocytosis by retinal pigmented epithelium that lacks myosin VIIa, the Usher syndrome 1B protein. Proc. Natl Acad. Sci. USA 2003;100:6481–6486. [PubMed: 12743369]
25. Libby RT, Steel KP. Electroretinographic anomalies in mice with mutations in Myo7a, the gene involved in human Usher syndrome type 1B. Invest. Ophthal. Visual Sci 2001;42:770–778. [PubMed: 11222540]

26. Self T, Mahony M, Fleming J, Walsh J, Brown SD, Steel KP. Shaker-1 mutations reveal roles for myosin VIIA in both development and function of cochlear hair cells. Development 1998;125:557–566. [PubMed: 9435277]
27. Truett GE, Heeger P, Mynatt RL, Truett AA, Walker JA, Warman ML. Preparation of PCR-quality mouse genomic DNA with hot sodium hydroxide and tris (HotSHOT). Biotechniques 2000;29:52–54. [PubMed: 10907076]
28. Dietrich WF, Miller JC, Steen RG, Merchant M, Damron D, Nahf R, Gross A, Joyce DC, Wessel M, Dredge RD, et al. A genetic map of the mouse with 4,006 simple sequence length polymorphisms. Nat. Genet 1994;7:220–245. [PubMed: 7920646]
29. Taylor BA, Navin A, Phillips SJ. PCR-amplification of simple sequence repeat variants from pooled DNA samples for rapidly mapping new mutations of the mouse. Genomics 1994;21:626–632. [PubMed: 7959741]
30. Manly KF, Cudmore RH Jr, Meer JM. Map Manager QTX, cross-platform software for genetic mapping. Mamm. Genome 2001;12:930–932. [PubMed: 11707780]
31. Johnson KR, Cook SA, Davisson MT. Chromosomal localization of the murine gene and two related sequences encoding high-mobility-group I and Y proteins. Genomics 1992;12:503–509. [PubMed: 1559701]
32. Hawes NL, Smith RS, Chang B, Davisson M, Heckenlively JR, John SW. Mouse fundus photography and angiography: a catalogue of normal and mutant phenotypes. Mol. Vis 1999;5:22. [PubMed: 10493779]
33. Hawes NL, Chang B, Hageman GS, Nusinowitz S, Nishina PM, Schneider BS, Smith RS, Roderick TH, Davisson MT, Heckenlively JR. Retinal degeneration 6 (rd6): a new mouse model for human retinitis punctata albescens. Invest. Ophthal. Visual Sci 2000;41:3149–3157. [PubMed: 10967077]
34. Weil D, Kussel P, Blanchard S, Levy G, Levi-Acobas F, Drira M, Ayadi H, Petit C. The autosomal recessive isolated deafness, DFNB2, and the Usher 1B syndrome are allelic defects of the myosin-VIIA gene. Nat. Genet 1997;16:191–193. [PubMed: 9171833]
35. Liu XZ, Walsh J, Mburu P, Kendrick-Jones J, Cope MJ, Steel KP, Brown SD. Mutations in the myosin VIIA gene cause non-syndromic recessive deafness. Nat. Genet 1997;16:188–190. [PubMed: 9171832]
36. Liu XZ, Walsh J, Tamagawa Y, Kitamura K, Nishizawa M, Steel KP, Brown SD. Autosomal dominant non-syndromic deafness caused by a mutation in the myosin VIIA gene. Nat. Genet 1997;17:268–269. [PubMed: 9354784]
37. Weil D, Blanchard S, Kaplan J, Guilford P, Gibson F, Walsh J, Mburu P, Varela A, Levilliers J, Weston MD, et al. Defective myosin VIIA gene responsible for Usher syndrome type 1B. Nature 1995;374:60–61. [PubMed: 7870171]
38. Bolz H, von Brederlow B, Ramirez A, Bryda EC, Kutsche K, Nothwang HG, Seeliger M, del CSCM, Vila MC, Molina OP, et al. Mutation of CDH23, encoding a new member of the cadherin gene family, causes Usher syndrome type 1D. Nat. Genet 2001;27:108–112. [PubMed: 11138009]
39. Bork JM, Peters LM, Riazuddin S, Bernstein SL, Ahmed ZM, Ness SL, Polomeno R, Ramesh A, Schloss M, Srisailpathy CR, et al. Usher syndrome 1D and nonsyndromic autosomal recessive deafness DFNB12 are caused by allelic mutations of the novel cadherin-like gene CDH23. Am. J. Hum. Genet 2001;68:26–37. [PubMed: 11090341]
40. Wilson SM, Householder DB, Coppola V, Tessarollo L, Fritzsch B, Lee EC, Goss D, Carlson GA, Copeland NG, Jenkins NA. Mutations in Cdh23 cause nonsyndromic hearing loss in waltzer mice. Genomics 2001;74:228–233. [PubMed: 11386759]
41. Ahmed ZM, Riazuddin S, Bernstein SL, Ahmed Z, Khan S, Griffith AJ, Morell RJ, Friedman TB, Wilcox ER. Mutations of the protocadherin gene pcdh15 cause usher syndrome type 1f. Am. J. Hum. Genet 2001;69:25–34. [PubMed: 11398101]
42. Alagramam KN, Yuan H, Kuehn MH, Murcia CL, Wayne S, Srisailpathy CR, Lowry RB, Knaus R, Van Laer L, Bernier FP, et al. Mutations in the novel protocadherin PCDH15 cause Usher syndrome type 1f. Hum. Mol. Genet 2001;10:1709–1718. [PubMed: 11487575]
43. Alagramam KN, Murcia CL, Kwon HY, Pawlowski KS, Wright CG, Woychik RP. The mouse ames waltzer hearing-loss mutant is caused by mutation of pcdh15, a novel protocadherin gene. Nat. Genet 2001;27:99–102. [PubMed: 11138007]

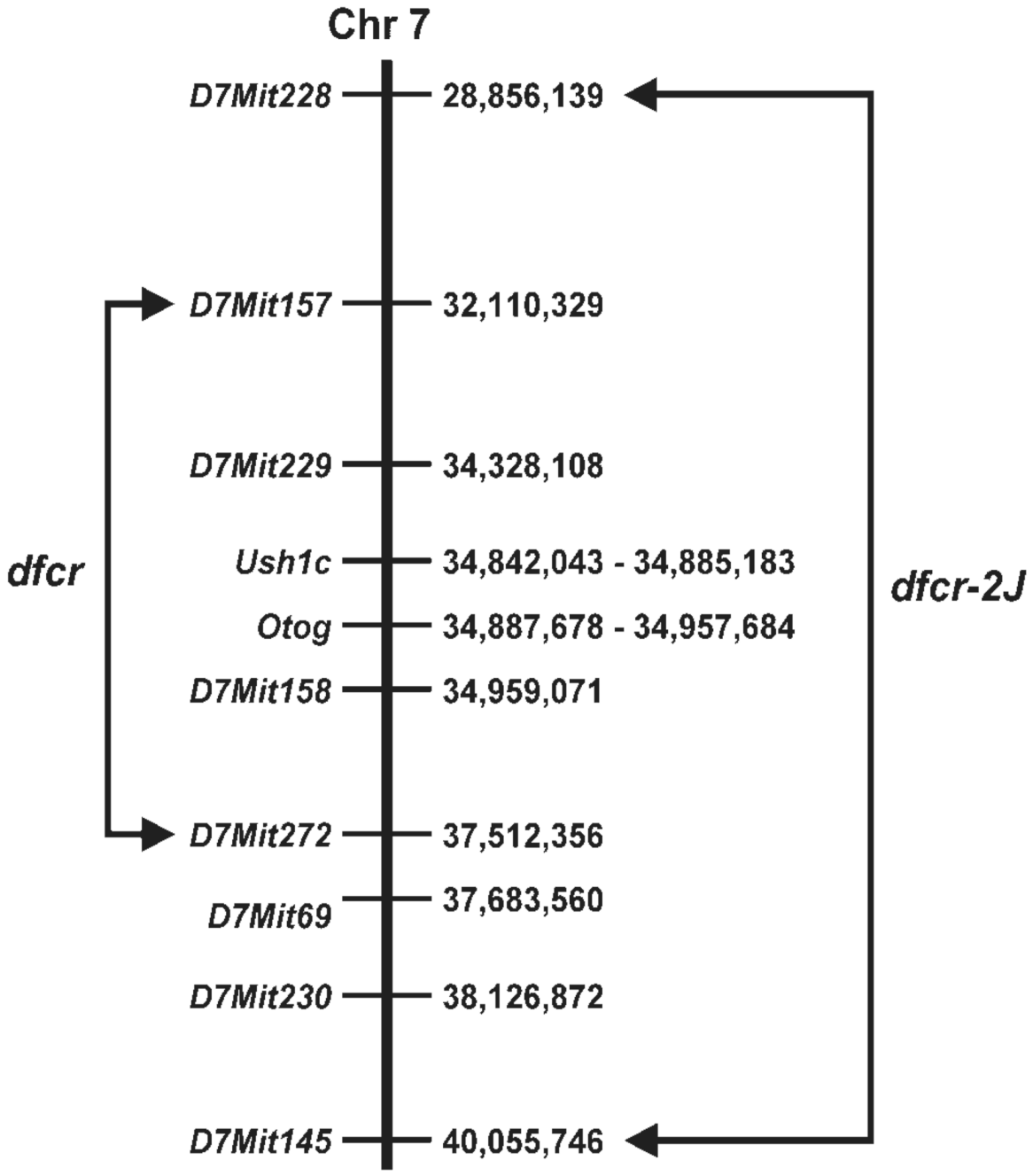

Figure 1.
Genetically derived candidate gene intervals for *dfcr* and *dfcr-2J*. The Ensembl base pair locations (from the NCBI 30 Mouse Genome Assembly, May 12, 2003) along Chr 7 are shown to the right of each marker and candidate gene. Arrows connect recombinant flanking markers for each linkage cross, delimiting the candidate gene intervals for each mutation.

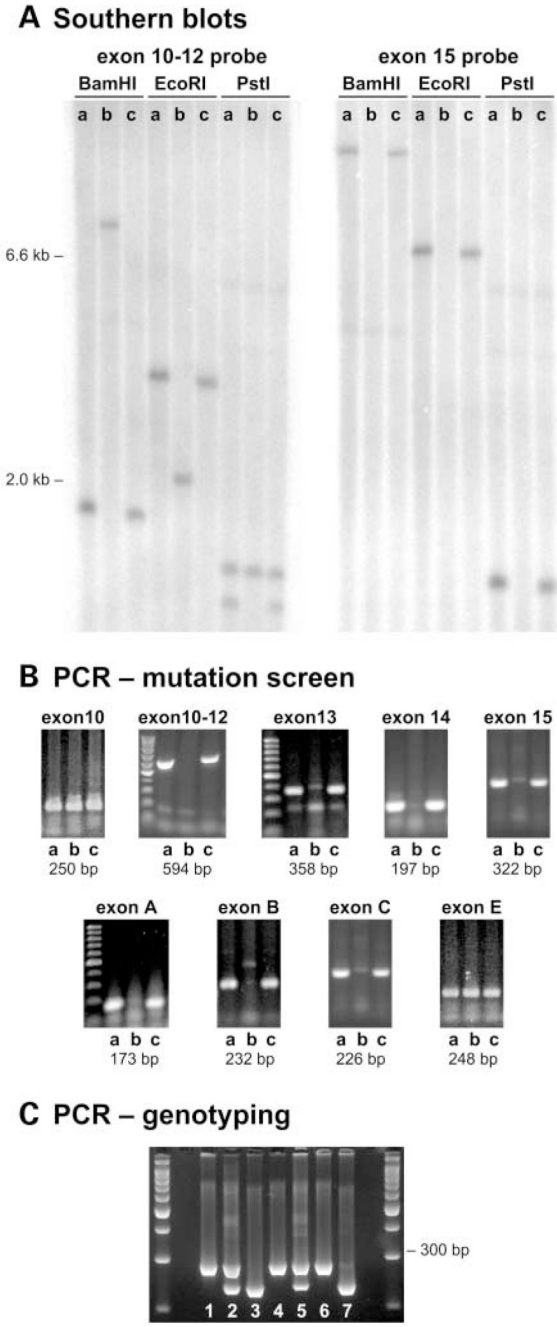

Figure 2.

The *dfcr* mutation of *Ush1c*. Genomic DNA samples from BALB/cByJ +/+control (lane a), *dfcr*/*dfcr* (lane b), and *dfcr-2J*/*dfcr-2J* (lane c) mice were compared. (**A**) Southern blot analysis. Restriction fragments from *dfcr*/*dfcr* mice are differently sized than those of controls and *dfcr-2J*/*dfcr-2J* mice when cDNA corresponding to exons 10–12 of *Ush1c* is used as a probe and absent when an exon 15 probe is used. (**B**) RT–PCR analysis. PCR primers flanking *Ush1c* exons 10–12, 13, 14, 15, A, B, and C amplified products with +/+ and *dfcr-2J*/*dfcr-2J* DNA but not with *dfcr*/*dfcr* DNA. Primers flanking exons 10 and E amplified products in all three DNA samples, indicating that the *dfcr* deletion lies between these two exons. (**C**) Genotyping mice with the *dfcr* mutation. Two primers flanking the deletion (in11-F and inD-

R, Table 2), amplify a 282 bp product only in mutant DNA. The in11-F primer and a primer within the deletion (ex12-R, Table 2), amplify a 234 bp product only in wildtype DNA. The three primers were used together in a single PCR reaction to amplify genomic DNA from +/+ (lanes 3 and 7), +/*dfcr* (lanes 2 and 5), and *dfcr*/*dfcr* (lanes 1, 4, and 6) mice. A 3% agarose gel was used to resolve the products shown here; the two outer lanes contain 100 bp size ladders.

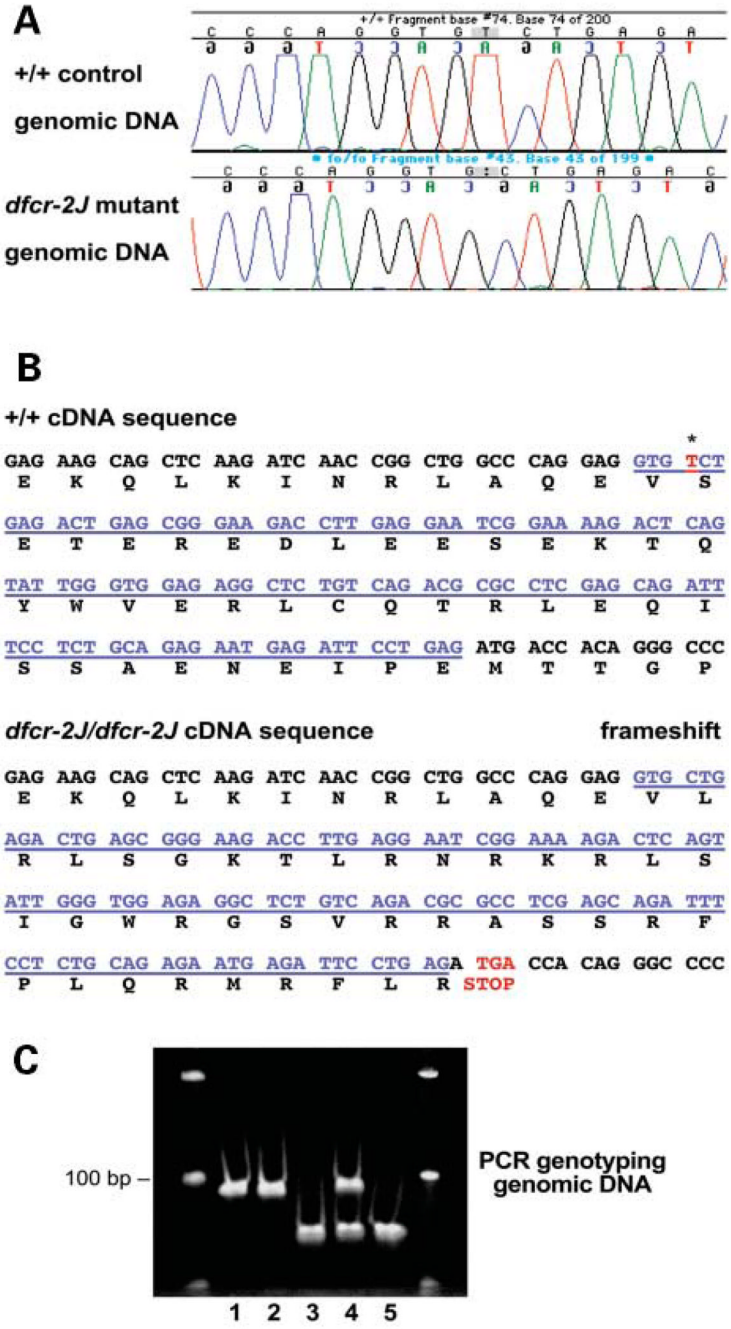

Figure 3.

The *dfcr-2J* mutation of *Ush1c*. (**A**) DNA sequence chromatogram of C57BL/6J +/+ control compared with homozygous *dfcr-2J* mutant, illustrating the deletion of a single bp (T/A) in mutant DNA. (**B**) The 1 bp deletion is at position 4 (indicated by an asterisk) of exon C (underlined in blue), which causes a frameshift and results in a transcription stop codon (shown in red) at the beginning of exon D. (**C**) Genotyping mice with the *dfcr-2J* mutation. Primers mutC-F and mutC-R, flanking the *dfcr-2J* mutation in exon C (Table 2), were used to amplify genomic DNA from +/+ (lanes 1 and 2), +/*dfcr-2J* (lane 4), and *dfcr-2J*/*dfcr-2J* (lanes 3 and 5) mice, progeny from matings between +/*dfcr-2J* parents. The reverse primer, mutC-R, ends immediately adjacent to the point of the 1 bp deletion in exon C. Two nucleotides in this primer

(underlined in Table 2) were changed (to GT from CA) to create an ApaL1 restriction site (GTGCAC) in mutant but not wildtype DNA. After incubation with the restriction endonuclease ApaL1, the wild-type 93 bp product is unaffected, whereas the mutant product is cleaved into 70 and 22 bp fragments. A 6% acrylamide gel was used to resolve the DNA fragments shown here; the two outer lanes contain 100 bp size ladders.

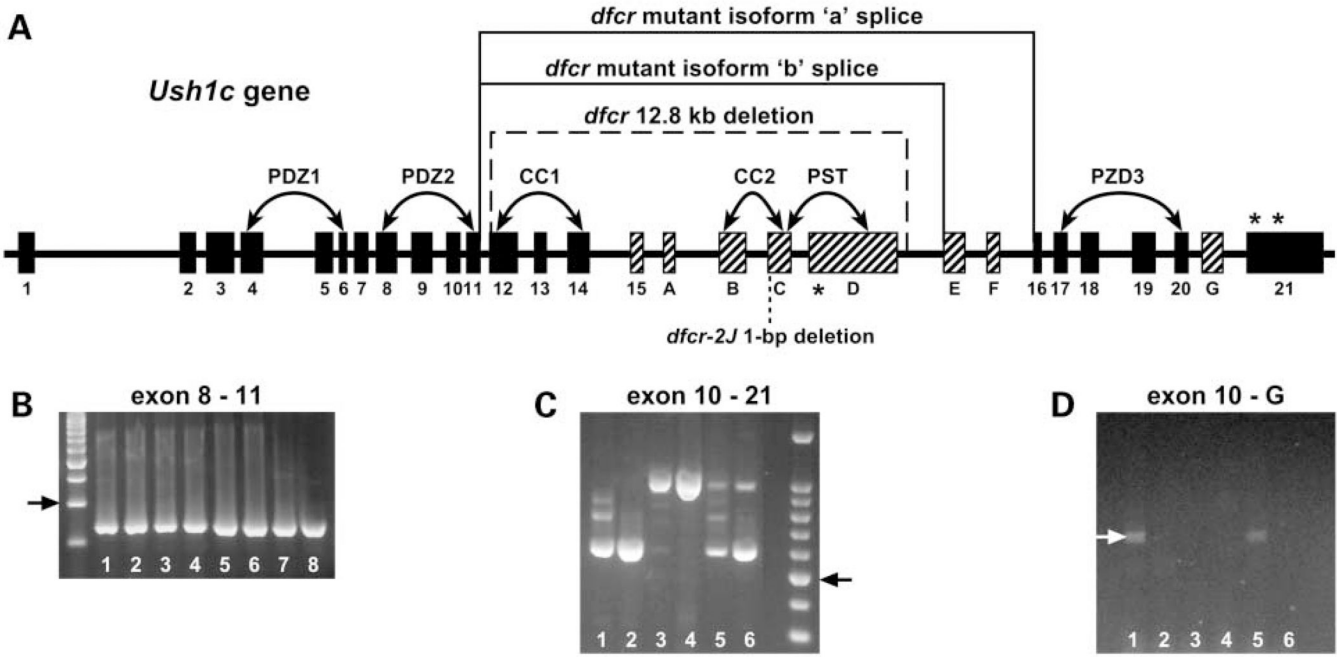

Figure 4.

Transcription of *dfcr* and *dfcr-2J* mutations. (**A**) *Ush1c* exon–intron structure. Exons are represented as rectangles and introns as lines. Exons (greatly exaggerated in size relative to introns) are designated according to Verpy *et al.* (4), with the 20 constitutive exons shown in black and the eight alternatively spliced exons in gray. A dashed line indicates the extent of the *dfcr* deletion and a dotted line marks the position of the *dfcr-2J* mutation. The *dfcr* deletion causes an inframe splicing of exon 11 with exon 16 in transcripts encoding the 'a' isoform of harmonin and an in-frame splicing of exon 11 with exon E in transcripts encoding the 'b' isoform. An asterisk in exon D marks the stop codon created by the *dfcr-2J* mutation, and asterisks in exon 21 denote the normal stop codons, unchanged by the *dfcr* mutation. Connected arrows indicate genomic regions encoding the PDZ, CC (coiled-coil), and PST (proline, serine, threonine-rich) domains of the harmonin protein. (**B**) *Ush1c* transcripts are detected in both *dfcr* and *dfcr-2J* mutant mice. The primers ex8-F (located within exon 8) and ex11-R (located within exon 11) amplified the expected 250 bp product in cDNA derived from inner ear (lanes 1–4) and kidney (lanes 5–8) of +/*dfcr* mice (lanes1 and 5), *dfcr*/*dfcr* mice (lanes 2 and 6), +/*dfcr-2J* mice (lanes 3 and 7), and *dfcr-2J*/*dfcr-2J* mice (lanes 4 and 8). Other tissues examined but not shown here (eye, brain, intestine) gave similar results. The arrow to the left of the figure indicates the position of the 300 bp DNA size marker. (**C**) Exons12, 13, 14 and 15 (396 nt) are deleted from isoform 'a' transcripts in *dfcr*/*dfcr* mice. The PCR products amplified with primers ex10-F (located within exon 10) and ex21-R (located within exon 21) from cDNAs derived from inner ear (lanes 1, 3 and 5) and intestine (lanes 2, 4 and 6) were smaller in *dfcr*/*dfcr* mice (574 bp; lanes 1 and 2) than those from +/+ mice (970 bp; lanes 3 and 4); both sizes were amplified in heterozygotes (lanes 5 and 6). Sequence analysis of the mutant 574 bp PCR product revealed an in-frame splicing of exon 11 with exon 16. The arrow to the right of the figure indicates the position of the 500 bp DNA size marker. (**D**) Exons 12, 13, 14, A, B, C and D (1137 nt) are deleted from isoform 'b' transcripts in *dfcr*/*dfcr* mice. A faint ~700 bp PCR product was amplified from inner ear cDNA with primers ex10-F and exG-R (located within exon G) of *dfcr*/*dfcr* (lane 1) and +/*dfcr* (lane 5) mice, but not from +/+ mice (lane 3) because of the large distance between exons 10 and G (>1800 nt) in wildtype cDNA. No product was amplified from intestine-derived cDNA of any genotype (lanes 2, 4 and 6). Sequence analysis

of the mutant product from inner ear (indicated by white arrow) revealed an in-frame splicing of exon 11 with exon E.

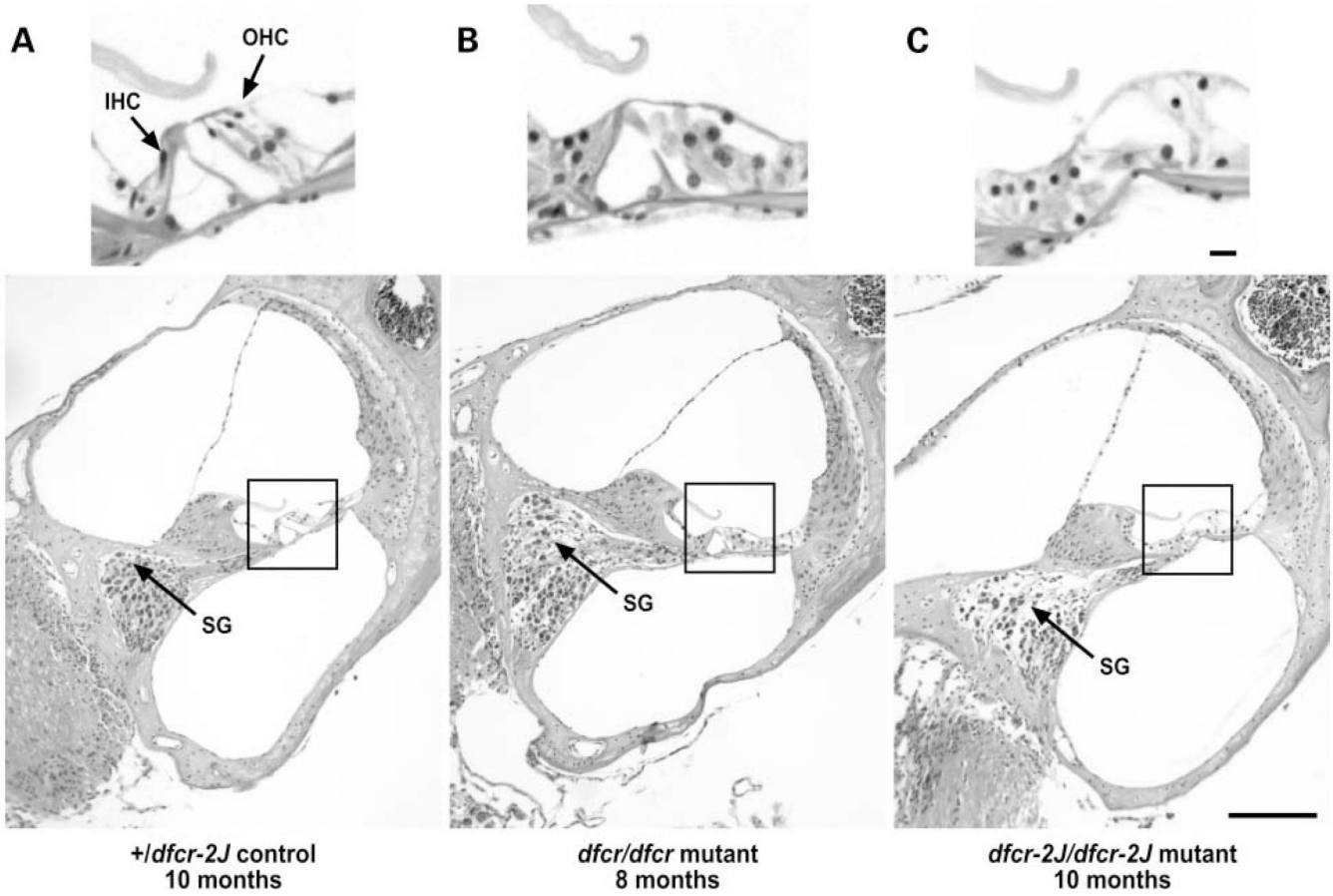

Figure 5.

Hair cell and spiral ganglion cell loss in cochleae of mutant mice. Cross sections through the basal turn of cochleae of a 10-month-old +/*dfcr-2J* control (**A**), an 8-month-old *dfcr*/*dfcr* mutant (**B**), and a 10-month-old *dfcr-2J*/*dfcr-2J* mutant (**C**). The upper panels show magnified images of the organ of Corti corresponding to the boxed areas in the lower panels. IHC, inner hair cell; OHC, outer hair cell; SG, spiral ganglia. Scale bars, 10 μm for upper panels and 100 μm for lower panels.

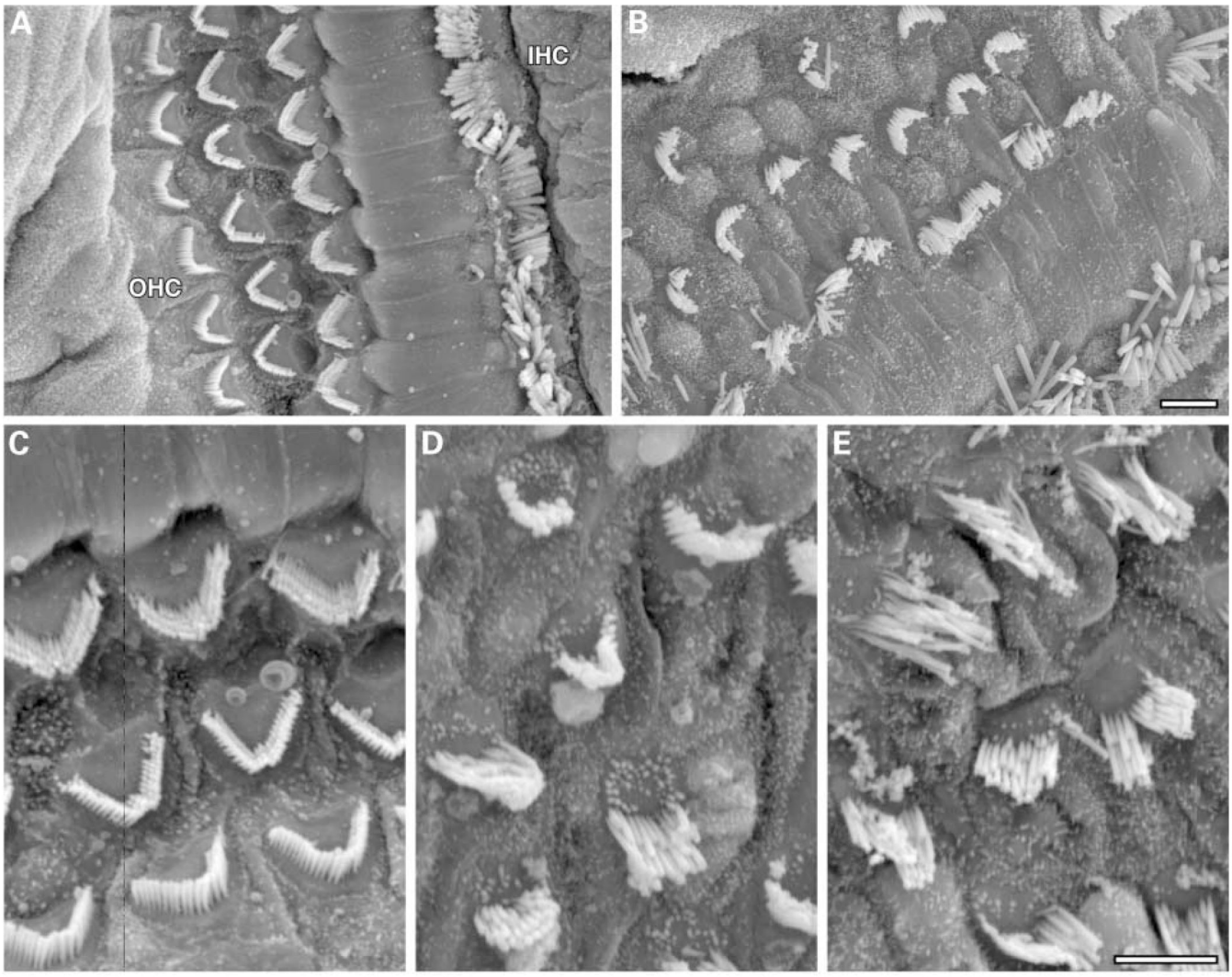

Figure 6.

Stereocilia disorganization in cochlear hair cells of mutant mice. Scanning electron micrographs of hair cell stereocilia in cochleae from 3-week old mice. The three rows of outer hair cells (OHC) and row of inner hair cells (IHC) in a cochlea from a +/*dfcr* heterozygous mouse (**A**) show a normal, highly organized pattern of stereocilia, as compared with stereocilia of a *dfcr*/*dfcr* mutant mouse (**B**). Scale bar, 5 μm. Hair cell loss in the mutant cochlea underlies the disrupted appearance of the hair cell pattern (B). Higher magnification of OHCs better illustrates the intricate pattern and rigid morphology of stereocilia of a normal mouse (**C**) compared with the disorganized and splayed stereocilia of *dfcr*/*dfcr* (**D**) and *dfcr-2J*/*dfcr-2J* (**E**) mutant mice. Scale bar, 5 μm.

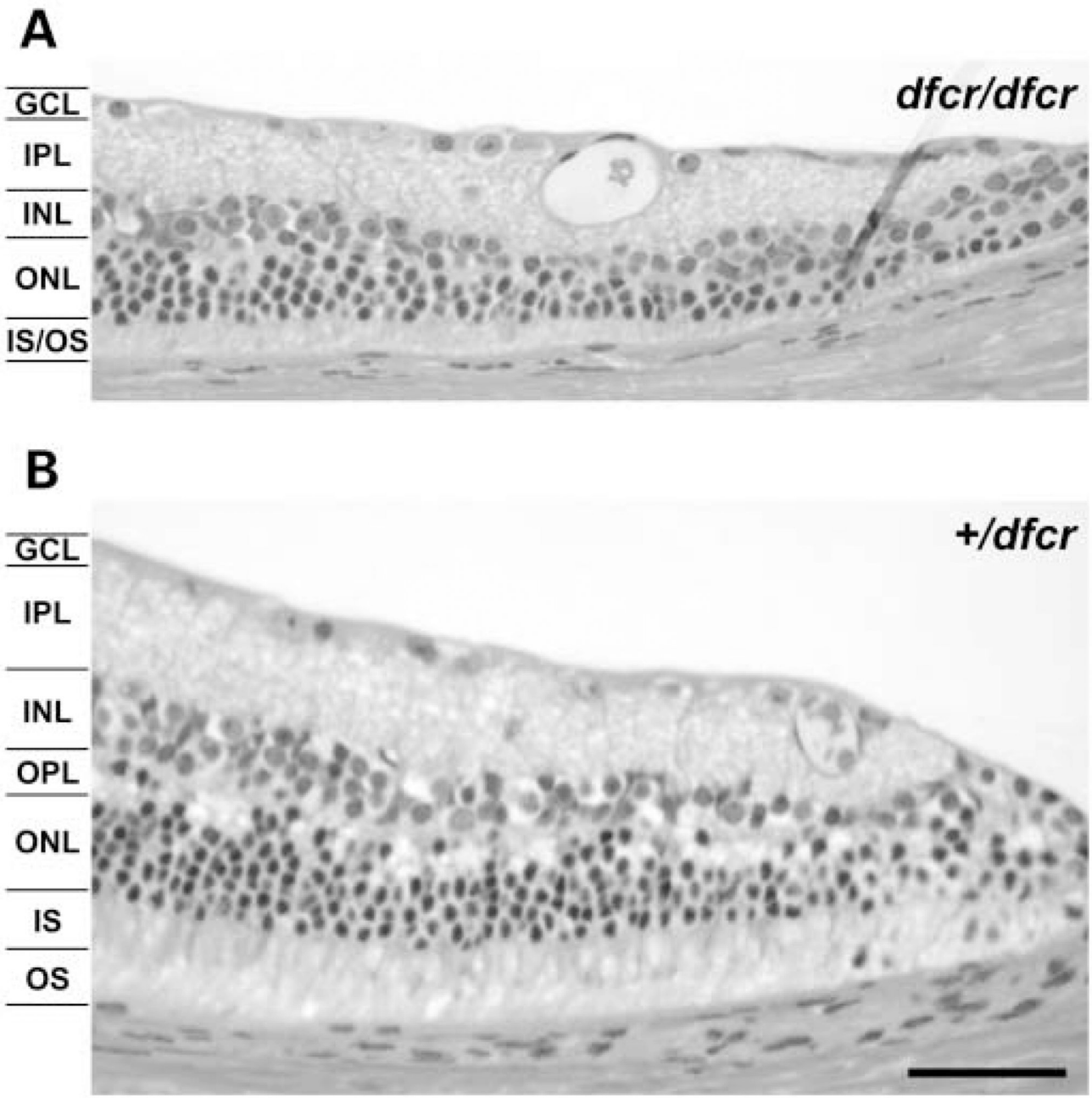

Figure 7.

Retinal histology of eyes from *dfcr* mutant mice compared with controls. Histologic sections of retinas from eyes of three BALB/cBy-*dfcr*/*dfcr* mutant mice showed evidence of a slight peripheral retinal degeneration at 9 months of age (**A**), compared with the normal retinal histology seen in eyes from three litter-mate BALB/cBy-+/*dfcr* controls (**B**). The overall thickness of cells at the periphery of the retina is reduced in mutant eyes compared with controls. Each layer is indicated as follows: ganglion cell layer (GCL), inner plexiform layer (IPL), inner nuclear layer (INL), outer plexiform layer (OPL), outer nuclear layer (ONL), inner segments (IS) and outer segments (OS). At about 200 μm from the outer edge of the retina, the

thickness of the INL-OS layers in mutant eyes was 40–80% that of normal eyes, and mutant eyes appeared to be missing the OPL. Scale bar, 50 μm.

Table 1

Mouse models for human Usher syndromes. Some of these same genes are also responsible for non-syndromic deafness (marked by asterisks)

Usher syndromes, type I	Locus	Gene (protein)	Human references	Mouse models (representative mutation)	Mouse references
USH1B	11q13	*MYO7A*	(34–37)	Shaker 1	(21)
DFNB2, DFNA11*		(myosin VIIa)		(*Myo7a*^{sh1})	
USH1C	11p15	*USH1C*	(3–6)	Deaf circler	This paper
DFNB18*		(harmonin)		(*Ush1c*^{dfcr})	
USH1D	10q21–q22	*CDH23*	(38,39)	Waltzer	(20,40)
DFNB12*		(cadherin 23)		(*Cdh23*^{v})	
USH1F	10q21–q22	*PCDH15*	(41,42)	Ames waltzer	(43)
		(protocadherin 15)		(*Pcdh15*^{av})	
USH1G	17q24–q25	*SANS*	(11)	Jackson shaker	(23)
		(sans)		(*Sans* ^{js})	

Table 2

PCR primers used in this study. Primers designated ‘fex’ are located in intronic sequences immediately flanking an exon, those designated ‘ex’ are located within exons, and those designated ‘in’ are located within introns. An ‘F’ indicates a forward primer and an ‘R’ a reverse primer relative to *Ush1c* transcription

Forward primer		Reverse primer		Product size (bp)
Mutation screening				
fex1-F	GTCCTGTCCTGGCAGCTAAC	fex1-R	GCCTCCACAGACCCTGTAAT	221
fex2-F	GATGTCTCCTCCCCAGGTCT	fex2-R	TGCCCACTCTGAATTCCTGT	268
fex3-F	CCACCCTCTGACATCTCCAA	fex4-R	CCCGCTCTGATGACTTACCT	435
fex5-F	CTGTGCCTGTTGCATCTCTC	fex7-R	TCCTTCTTCAAGGCCAGCTA	547
fex8-F	GGCCACTTGAAGGCATGTAG	fex8-R	TTGACCAGCTGTCACTGAGC	225
fex9-F	CAGAAGGCTACAGGCTGGTC	fex9-R	GACGCAGCATCTGTCAGTGT	247
fex10-F	CTGTGGGATCACTGGCCTAT	fex10-R	CTGGAAGACGTGTGTGGAGA	250
fex10-F	CACACACTGACCCGTTTTTCT	fex12-R	TCAGTTGTGTCTGGTGTGGAA	594
fex13-F	CAGAACCACACCCACAGTTG	fex13-R	GGTGGATTTGAGCCAATGAA	358
fex14-F	AGGTTCTGCCATCAATCACA	fex14-R	ATCCCGGACAGGTCATACAT	197
fex15-F	CACACCAGAGCAAGGAGACC	fex15-R	ATGGTCCAGCTCTTTCAAGC	322
fex16-F	CCATCCCAACCACAGCTACT	fex16-R	CCCTCTGAGCTGGAGAGTTC	221
fex17-F	AGGCCACACATGCTCTTACC	fex17-R	AGGGAACCAAGACGACAGAG	178
fex18-F	CTATCTGTGTGGCTGCCTGA	fex18-R	TCTGCTCTCCTGGGACATCT	212
fex19-F	GAGTCAGGCACAGGTCACAA	fex19-R	TTGTAAGGCCAGGGTCTGAG	225
fex20-F	GTCAGAACACCAGGCAGGTT	fex20-R	GGACATCCCTTTCCCTGAAT	220
fex21-F	GCAAGTCCTGTCCACTCCAT	fex21-R	TGCTGTCCACACAATTCACC	454
fexA-F	ACATACCTTGGGAACGCAAC	fexA-R	CACATCAAACTTGGCAGCAC	173
fexB-F	CACAATGCTCCATCTGCTCA	fexB-R	ATCTGGCCCTTGGAGGTATG	232
fexC-F	TACCCATGTGACTCGGTGTG	fexC-R	GTGACTGTCAGGAGGGTCCA	226
fexD-F	GGATCCAGCAGCAAGAGAAA	exD-2R	CGGGTAGGAGTGAGGTCTTG	413
exD-2F	CACACCACTGACCTGGATGA	fexD-R	CTTCCTTTGCAAGCACAACA	437
fexE-F	ATGACGCCACATGGGTATCT	fexE-R	TCACTTCCCTTCCAGAGGTG	248
fexF-F	CCGAACATCAGCCTATCTGG	fexF-R	CCAGACACACGGGTCTCATT	202
fexG-F	CCTCTTGTCTCCTGCTCCAC	fexG-R	CCAGTCCAAAGAACCTCCAG	227
dfcr genotyping				
In11-F	GAGCCGTAAGTCCAGAATGC	ex12-R	TGCTCCTGGAGGATCTTGTT	
		inD-R	TCATCAGAGGCTGCTGACAC	
dfcr-2J genotyping				
mutC-F	TACCCATGTGACTCGGTGTG	mutC-R	AAGGTCTTCCCGCTCAGTCT**GT**G	
Transcription analysis				
ex8-F	CGGACAACCAAGGAGAAGAA	ex11-R	GGCTGCTCTTCAGGACATTC	
ex10-F	ACTTCACCAACCTGGACCAC	exG-R	GCTGCAGGAAAAACCCGTGTCT	
		ex21-R	TGTGGGTCAGCTTCCAGGGAGACTTT	

Table 3

ABR thresholds of mutant and control mice. The number, gender (f = female, m = male), and ages of mice tested are given for each genotype. ABR threshold values below 55 (click, 8 kHz) 35 (16 kHz) or 60 (32 kHz) are considered within the normal range for mice. The maximum amplitude presented for each test stimulus was 100 dB

Genotype	Number	Age (days)	Average ABR thresholds (dB SPL)			
			Click	8 kHz	16 kHz	16 kHz
dfcr/+	7 (4 f, 3 m)	21–176	37	46	21	50
dfcr/*dfcr*	8 (4 f, 4 m)	21–82	100	100	100	100
dfcr-2J/+	4 (3 f, 1 m)	98	40	50	20	50
dfcr-2J/*dfcr-2J*	2 (2 f)	98	100	100	100	100